this monochromator and detector in a phosphorescence-lifetime experiment (*6*).

We provide our students with an extensive description of the experiment, including operating instructions and listings of the data-acquisition and data-analysis computer programs. Copies of this material, either on paper or WordPerfect 5.1 floppy disk, are available at no cost from the author.

Acknowledgment

Financial support from a Kresge Foundation grant is gratefully acknowledged.

Literature Cited

1. Muenter, J. S.; Deutsch, J. L. *J. Chem. Educ.* **1994**, 580–585 (the next paper).
2. (a.) Schwenz, R. W.; Moore, R. J. *Physical Chemistry: Developing a Dynamic Curriculum*; ACS: Washington, DC, 1993; Chapters 6–13; (b.) Galloway, D. B.; Clolkoowski, E. L.; Dallinger, R. F. *J. Chem. Educ.* **1992**, *69*, 79–83; (c.) Erskine, S. R.; Bobbit, D. R. *J. Chem. Educ.* **1989**, *66*, 354–357; (d.) Jones, B. T.; Smith, B. W.; Leong, M. B.; Mignardi, M. A.; Winefordner, J. D. *J. Chem. Educ.* **1989**, *66*, 357–358; (e.) King, M. E.; Pitha, R. W.; Soutum, S. F. *J. Chem. Educ.* **1989**, 66, 787–790; (f.) Hughes, E., Jr.; Jelks, V.; Hughes, D. L. *J. Chem. Educ.* **1988**, 65, 1007–1008.
3. Sakurai, K; Broida, H. P. *J. Chem. Phys.* **1970,** *53,* 1615–1616.
4. Herzberg, G. *Spectra of Diatomic Molecules*; van Nostrand: Princeton, 1950.
5. Shoemaker, D. P.; Garland, C. W.; Nibler, J. W. *Experiments in Physical Chemistry,* 5th ed.; McGraw–Hill: New York, 1989.
6. Dyke, T. R.; Muenter, J. S. *J. Chem. Educ.* **1975**, *52*, 251–258.

The Nitrogen-Laser Excited Luminescence of Pyrene

A Student Laboratory Study of Excimer Dynamics

John S. Muenter
University of Rochester, Rochester, NY 14627

John L. Deutsch
State University of New York, Geneseo, NY 14454

An undergraduate laboratory experiment that uses a nitrogen laser to produce the first excited singlet state of pyrene is described. The resulting luminescence is studied as a function of wavelength, time, and pyrene concentration to observe the dynamics of both the excited pyrene monomer and the pyrene excimer. The initial rise and subsequent decay of the excimer is directly observed. Data is analyzed in terms of coupled rate equations, and students obtain four different rate constants in interactive calculations. The apparatus is relatively easy to set up, and it introduces students to a variety of topics in photochemical kinetics and fast-measurement techniques.

The origins of physical chemistry were based on the need to understand the rates and mechanisms of chemical reactions. Investigating ever-faster processes is a continuing feature in the study of chemical kinetics and dynamics. In recent years, advances in lasers, electrooptics, and electronics have extended chemical measurements from nanosecond to femtosecond time regimes (*1*). Some of these same developments also make it perfectly feasible to observe nanosecond processes in undergraduate teaching laboratories. This paper describes the second of two student laboratory projects that introduce basic laser techniques into physical chemistry laboratories. The first of these two experiments (*2*) focuses on molecular spectroscopy and studies the rotationally resolved laser-induced fluorescence spectrum of molecular iodine. These two experiments join a relatively small group of laser-based undergraduate laboratory projects (*3*); some are cited in ref *3*. The present paper concentrates on fast kinetics measurements using a pulsed laser.

An ideal kinetics scheme for a student laboratory contains competitive first- and second-order reactions, and involves a reactive intermediate species. Monitoring the time and concentration dependence of reactants and products provides the necessary insight to understand both mechanisms and rates. The reaction dynamics of the first excited singlet state of pyrene provides these features, along with the advantages of laser initiation and optical detection. Students observe the time dependence of fluorescence from electronically excited pyrene and also from the pyrene excimer. Fluorescence signals, including those from the initial rise and then decay of the excimer concentration, are quantitatively measured and analyzed. The kinetic scheme is described by straightforward rate equations, but the coupling of these equations leads to moderately complicated time dependence of the chemical concentrations involved. In particular, students directly observe that not all radiative processes exhibit the simple exponential decay that results from first-order kinetics.

Pyrene: Its Luminescence and Excimer Formation

Pyrene is a planar aromatic hydrocarbon; its structure is shown in Figure 1. It is moderately soluble in common solvents, and the work described here is done in cyclohexane solution. The 337-nm radiation from a nitrogen laser excites the S_0 ground electronic state to the first excited singlet state, S_1. The resulting luminescence is quite intense and easily detected by eye, but this emission is not simple fluorescence (*4*).

Complex Radiative Decay

The complexity of pyrene's radiative decay is evidenced: It is both nonexponential in time and strongly concentration-dependent. Even simple visual inspection of the luminescence indicates unusual behavior. Emission from a 10^{-2} M pyrene solution is blue–green (peaking at about 500 nm), whereas a 10^{-6} M solution produces blue–violet emission (having a 390-nm maximum). These features suggest more than one active chemical species.

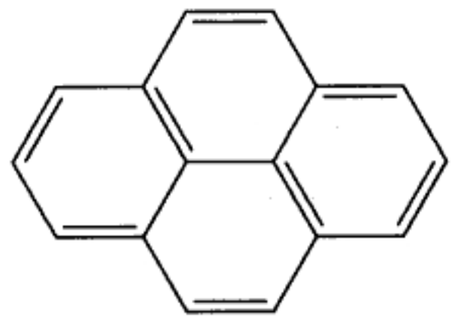

Figure 1. The structure of pyrene.

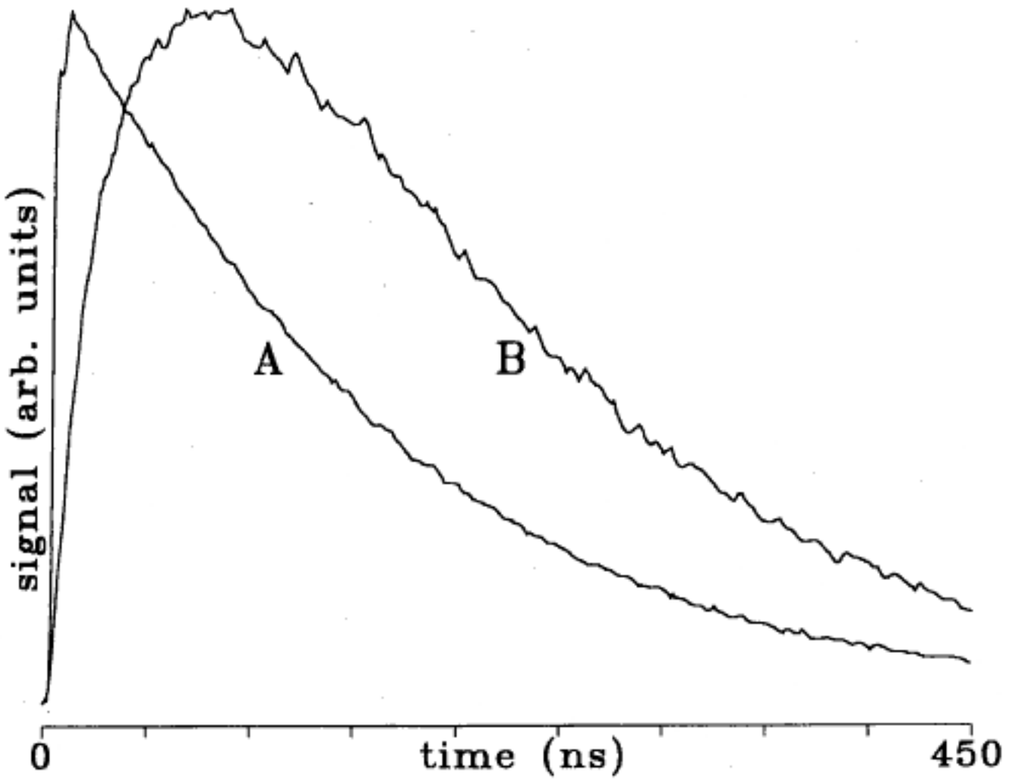

Figure 2. The time-resolved luminescence of a 10^{-3} M solution of pyrene, following nitrogen-laser excitation. Curve A was detected at 400 nm, and curve B was detected at 500 nm.

Excimer Formation

This experiment and the accompanying analysis demonstrate that electronically excited pyrene molecules, P^*, react with ground-state pyrene, P, to form an excited state dimer, PD^*, commonly called an excimer. We will use the notation P and P^* to signify the ground and excited state of pyrene monomer, and PD and PD^* for the ground and excited state of pyrene dimer. PD^* will also be called the pyrene excimer.

The important reactions involved in this experiment are

$$P + h\nu \rightleftarrows P^* \quad (1)$$

$$P^* + P \rightleftarrows PD^* \quad (2)$$

$$PD^* \rightleftarrows PD + h\nu \quad (3)$$

In a dilute solution, P^* does not encounter a P during its radiative lifetime, and the short-wavelength, blue–violet emission is P^* fluorescence. This is confirmed by observing simple exponential decay from a 10^{-6} M solution. In a 10^{-2} M solution, PD^* formation competes effectively with P^* fluorescence, and the observed luminescence is dominated by the radiative decay of PD^*, described by eq 3 (*5*). The longer wavelength of the PD^* fluorescence is a measure of the stabilization energy of the excimer, relative to a separated P, P^* pair. This stabilization arises from the delocalization of the excitation over both of the pyrene molecules. The time dependence of the P^* and PD^* emissions can be followed independently by wavelength; this resolves the luminescence. This is shown in Figure 2, which contains experimental data for a 10^{-3} M sample. Curve A was recorded at 400 nm, whereas curve B represents 500-nm data. The initial rise and subsequent decay of the PD^* concentration is clear.

Various Reaction Channels

A relatively large number of rate constants affect $[P^*]$ and $[PD^*]$, that is, the concentrations of P^* and PD^* after the laser excitation pulse. The various reaction channels are discussed in ref *4* and shown schematically in Figure 3. The fluorescence and first-order nonradiative relaxation of P^* back to P are determined by k_{FM} and k_{NM}, where the subscript M signifies monomer rate constants. Similarly, the decay of the excited dimer, or excimer, is described by k_{FD} and k_{ND}. The second-order excited monomer to excimer reaction is characterized by $k_{MD}[P]$, where the MD subscript implies monomer to dimer. The excited dimer to excited monomer reaction is first-order, with rate constant k_{DM}.

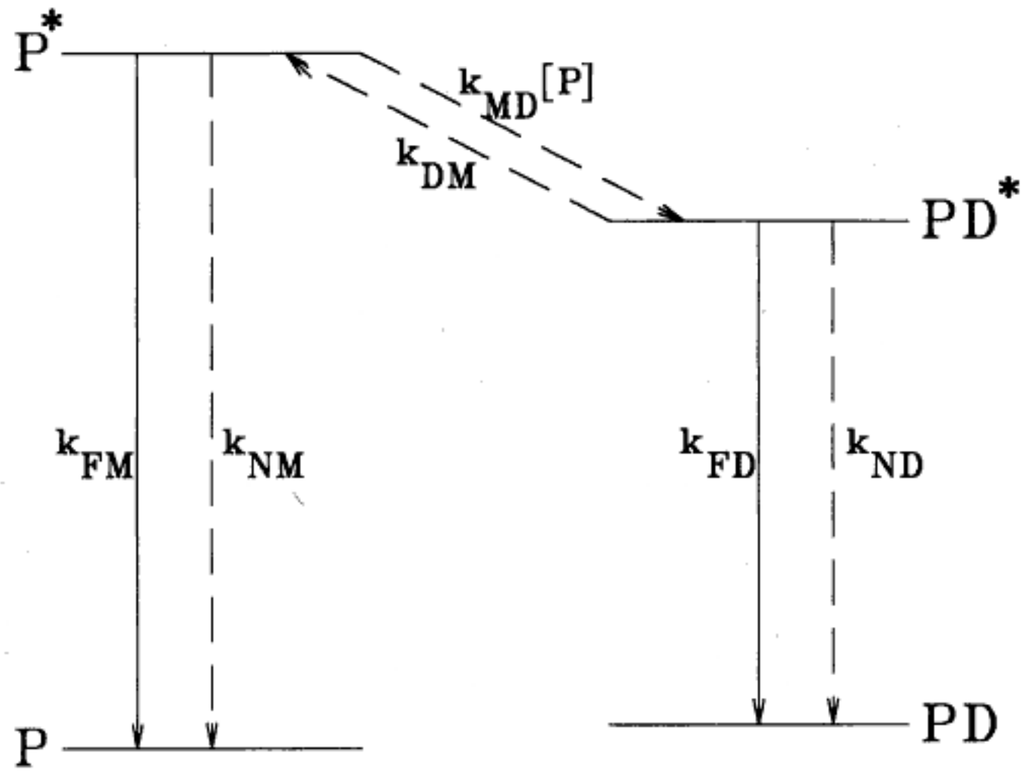

Figure 3. Schematic energy levels and rate processes associated with pyrene luminescence.

The various sources and sinks for P^* and PD^* shown in Figure 3 makes it straightforward to write the differential equations describing the time-dependent concentrations of $[P^*]$ and $[PD^*]$ (*4*):

$$\frac{d[P^*]}{dt} = -\left(k_{FM} + k_{NM} + k_{MD}[P]\right)[P^*] + k_{DM}[PD^*] \quad (4)$$

$$\frac{d[PD^*]}{dt} = -\left(k_{FD} + k_{ND} + k_{DM}\right)[PD^*] + k_{MD}[P][P^*] \quad (5)$$

It is not possible to separate the effect of k_{FM} from k_{NM}, or the effect of k_{FD} from k_{ND}, in the experiment described here, so it is useful to define

$$k_M \equiv k_{FM} + k_{NM} \quad (6)$$

$$k_D \equiv k_{FD} + k_{ND} \quad (7)$$

With these definitions, eqs 4 and 5 simplify to

$$\frac{d[P^*]}{dt} = -\left(k_M + k_{MD}[P]\right)[P^*] + k_{DM}[PD^*] \quad (8)$$

$$\frac{d[PD^*]}{dt} = -\left(k_D + k_{DM}\right)[PD^*] + k_{MD}[P][P^*] \quad (9)$$

Because $[P^*]$ and $[PD^*]$ each appear in both rate equations, eqs 8 and 9 are coupled and cannot be solved independently. A rather complicated, but analytic, solution exists for eqs 8 and 9 (*4*, *6*).

$$[P^*] = \left(\frac{\lambda_2 - X}{\lambda_2 - \lambda_1}\right)\left(e^{-\lambda_1 t} + \left(\frac{X - \lambda_1}{\lambda_2 - X}\right)e^{-\lambda_2 t}\right) \quad (10)$$

$$[PD^*] = \left(\frac{k_{MD}[P]}{\lambda_2 - \lambda_1}\right)\left(e^{-\lambda_1 t} - e^{-\lambda_2 t}\right) \quad (11)$$

where

$$X \equiv k_M + k_{MD}[P]$$

$$Y \equiv k_D + k_{DM}$$

$$R \equiv \left((Y - X)^2 + 4k_{MD}k_{DM}[P]\right)^{1/2}$$

$$\lambda_1 \equiv \tfrac{1}{2}(X + Y - R)$$

and

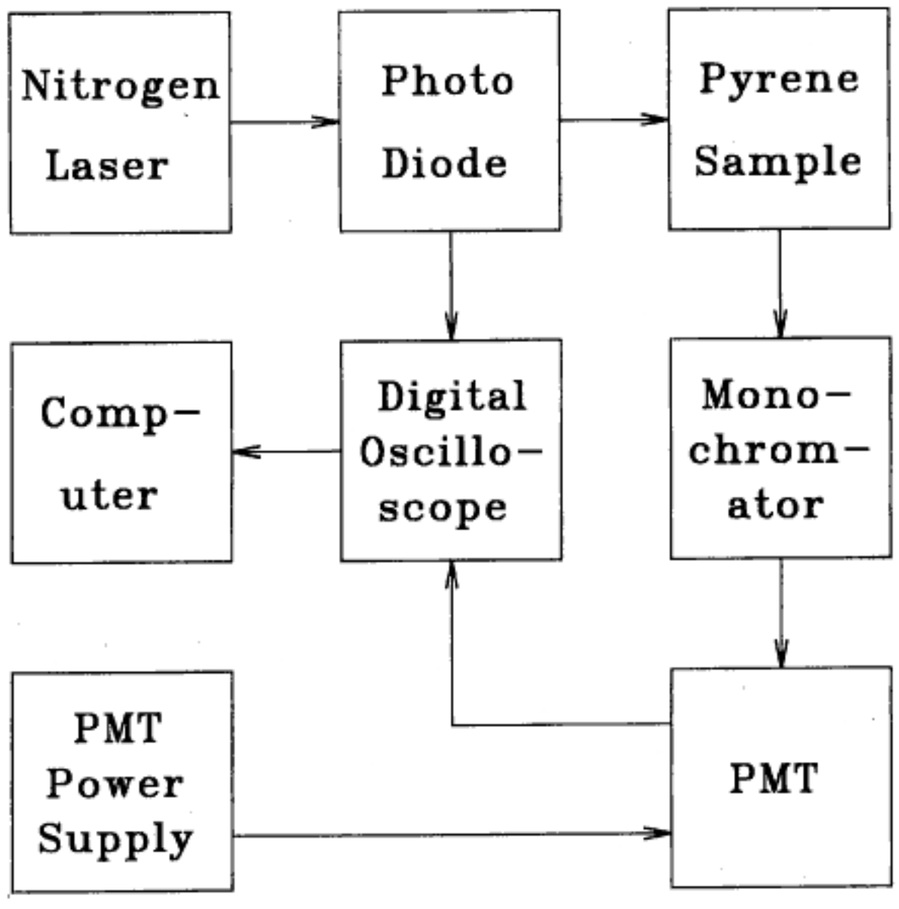

Figure 4. A block diagram for the pyrene luminescence apparatus.

Table 1. Sources and Components Used

Component	Manufacturer	Model No.
N_2 Laser	Laser Photonics	LN203C
Photodiode	Thorlabs	DET2-Si
Monochromator	SPEX	340S
PMT	RCA	IP28
PMT Housing	Products for Research	PR-1405-RF
PMT Power Supply	Hewlett–Packard	6515A
Oscilloscope	Hewlett–Packard	54510B
Cables	Pasternack	RG142B/U
50-Ω Termination	Pasternack	PE6008-50

$$\lambda_2 \equiv \tfrac{1}{2}(X + Y + R)$$

This situation also provides an excellent opportunity for students to numerically solve coupled differential equations. Students can easily write concentrations at increment $n + 1$, $[P^*]_{n+1}$, and $[PD^*]_{n+1}$, in terms of $[P^*]_n$ and $[PD^*]_n$ by dividing the observation time period into a large number of increments, δt. The differential changes in $[P^*]$ and $[PD^*]$ are found by multiplying eqs 8 and 9 by dt. Equating dt with the time increment δt gives

$$[P^*]_{n+1} = [P^*]_n + \left(k_{DM}[PD^*]_n - k_M[P^*]_n - k_{MD}[P][P^*]_n\right)\delta t \quad (12)$$

$$[PD^*]_{n+1} = [PD^*]_n + \left(k_{MD}[P][P^*]_n - k_D[PD^*]_n - k_{DM}[PD^*]_n\right)\delta t \quad (13)$$

Fixing $[P^*]_0 = 1$ and $[PD^*]_0 = 1$, choosing $\delta t = 10^{-9}$, and using double precision arithmetic gives results indistinguishable from those produced by eqs 8 and 9. Rate constants are determined by displaying calculated and observed emission curves, and then adjusting the four rate constants to produce the best agreement for a given concentration.

Experimental Procedure

Apparatus

The experimental apparatus is shown schematically in Figure 4. The specific components used are listed in Table 1. Briefly, the experiment proceeds as follows. The pyrene sample is excited by a pulse of UV light from a nitrogen laser. Scattered laser light illuminates a fast photodiode, which generates a trigger pulse to initiate data acquisition by a digital oscilloscope. The pyrene luminescence is wavelength-analyzed with a monochromator and detected with a photomultiplier tube (PMT). The PMT signal is displayed on the digital oscilloscope; from it, data are transferred to a personal computer (PC) for analysis.

Almost any N_2 laser can be used for this project. The one used here produces 100 μJ in pulses having 600-ps full widths at half-height. This narrow pulse width is convenient, but not essential. (The affects of broader laser pulses will be dealt with in the Analysis section.) The space between the laser output port and the sample block is enclosed with a piece of PVC pipe to keep scattered laser light from entering the laboratory. The photodiode is mounted at a small hole drilled in this pipe. The photodiode is contained in a compact housing, complete with on/off switch, connector, and battery; it has a rise time of less than 1 ns.

The only major components that are not commercially available are the pyrene samples and sample housing. Samples are housed in a simple aluminum block, bolted to the monochromator slit assembly. The sample is placed in a vertically bored hole; horizontal ports for the laser light and the luminescence are at right angles. A third horizontal port, opposite the luminescence port, is used to visually observe the sample. The pyrene samples are contained in 10-mm-diameter pyrex tubes. A 10^{-2} M solution of pyrene (Aldrich 18,551-5 in spectroscopic-grade cyclohexane) was made up, and then consecutive dilutions were carried out for 10^{-3}, 10^{-4}, 10^{-5}, and 10^{-6} M samples. Each sample was vacuum-degassed using several liquid nitrogen freeze–thaw cycles, and then sealed off with a glassblowing torch. The vacuum degassing is essential, and some care is required to avoid contamination of the samples on the vacuum system. For example, the first set of samples made up for this experiment was not satisfactory due to a strongly fluorescing Apiezon grease impurity. Switching to silicon grease minimized this problem.

The same monochromator used in the I_2 laser-induced fluorescence experiment (*1*) is used here, but with 5-nm band pass. Almost any monochromator will adequately separate the 400- and 500-nm signals. We have carried out this experiment using interference filters to block laser scatter and select either the P^* or PD^* fluorescence. In this configuration, which lowers the apparatus cost significantly, a filter holder fits between the PMT housing and the sample block. An Oriel Model 52053 long-pass filter-block laser scatter, and either an Edmunds Model N43,104 or N43,117 band-pass filter selects the fluorescence wavelength.

The dynode structure of the 1P28 PMT produces a rise time of about 2 ns, and almost any PMT of this type can be used. This is demonstrated here by using an old, authentic RCA 1P28. However, it is important to use a 50-Ω termination at both the PMT housing and the oscilloscope input in order to avoid slow response associated with charging and discharging the cable capacitance. The type of cables used to connect the PMT to the dc power supply and oscilloscope also proves to be important. Nitrogen lasers are infamous for generating electronic interference, and this was indeed a problem here when ordinary coaxial cables were used. Switching to double-shielded cables completely eliminated this problem, even when using 5-mV/div oscilloscope sensitivity.

The digital oscilloscope used here has a 300-MHz bandwidth and 1-ns rise time; it records data at 1-ns intervals. This level of performance is convenient, but not essential. Because the signal is repetitive, a lower sampling-rate instrument can be used as long as an about 100-MHz bandwidth and about 3-ns rise time are available for repetitive signals. This has been demonstrated using a Hewlett–Packard Model 54600A oscilloscope. Approximately 50 laser pulses are required to acquire each waveform, but this still requires just a few seconds. Precautions needed to analyze data acquired with broader laser pulses or slower-responding instrumentation are discussed below. Data is transferred from the oscilloscope to the PC using the program SCOPELNK (Hewlett–Packard).

Table 2. Experimental Parameters

–log [P]	λ	mV/div	ns/div	V_{PMT}
2	400	10	50	410
2	500	10	50	390
3	400	10	50	340
3	500	10	50	420
4	400	10	100	320
4	*500*	10	100	480
5	400	10	200	340
5	500	10	200	630
6[a]	400	10	200	430

[a]The 10^{-6} M sample exhibits no excimer signal.

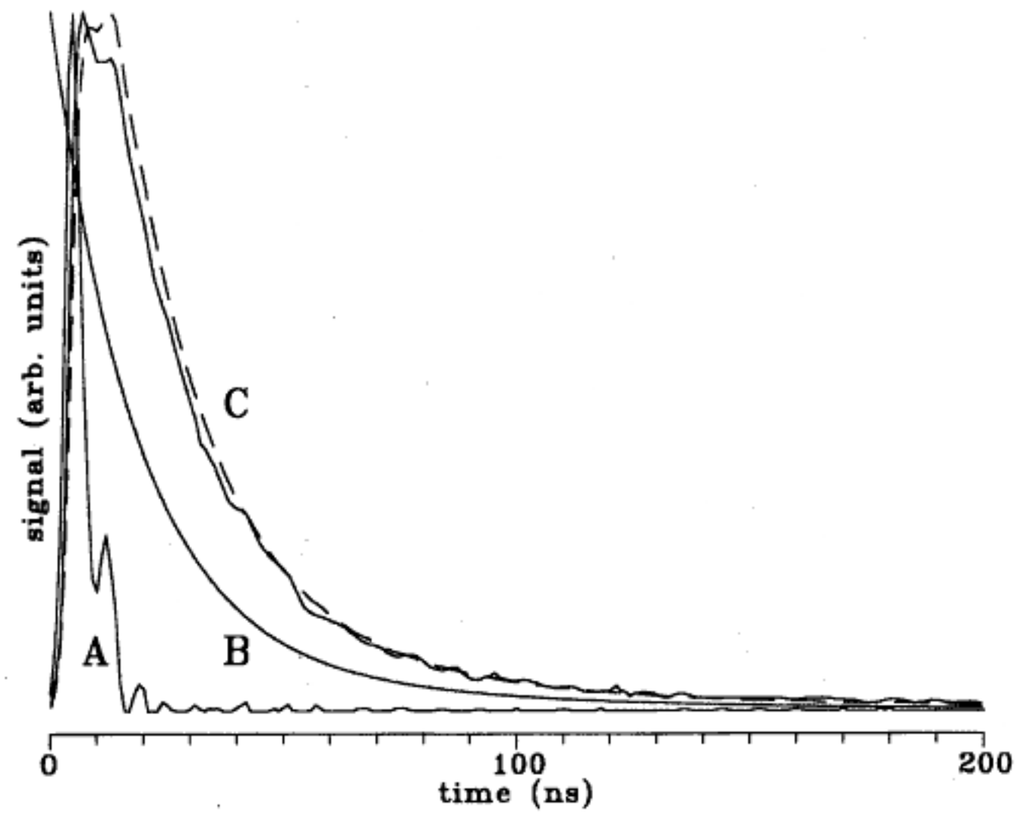

Figure 5. Various signals associated with this experiment are (A) Experimental response of PMT to scattered laser light, (B) calculated P^* fluorescence for 10^{-2} M pyrene, (C, solid) observed P^* fluorescence for 10^{-2} M pyrene, (C, dashed) convolution of A and B.

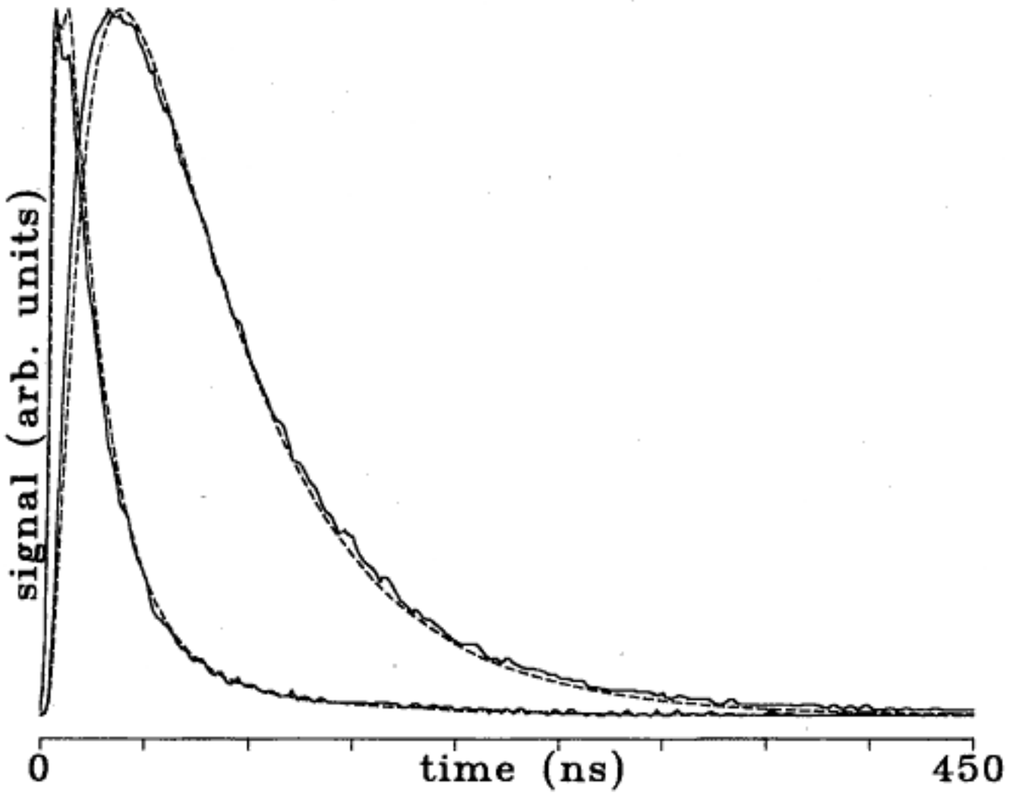

Figure 6. Observed (solid lines) and calculated (dashed lines) P^* and PD^* fluorescence for 10^{-3} M pyrene.

Procedure

We use this experiment to demonstrate laser safety, as well as to study the photophysics and photochemistry of pyrene.

- *Safety*: General information on laser safety can be found on page 125 of ref *3*, and information specific to nitrogen lasers is on page 116. In its normal configuration, the apparatus completely encloses the laser radiation, and eye protection is not necessary. To insure safe operation, the sample block has a cover that is interlocked with the laser, so laser operation is stopped if the cover is not properly closed. However, it is also desirable for students to see the luminescence to observe the concentration-dependent color, so a small viewing port, opposite the monochromator slits, is provided. When this port is in use, students wear goggles that attenuate UV radiation by 10^4 (Oriel 49126).

It is also quite easy to see the changes in optical density of the samples as different concentrations are observed. To aid this aspect of the experiment, the laser beam is collimated by incorporating two lenses and two diaphragms into the PVC pipe connecting the laser to the sample block. The lenses form a telescope, and their position is adjusted so that the laser beam has a long focal waist centered at the sample position. The diaphragms minimize scattered light, and the light beam in the sample is essentially collimated. The 1/*e* absorption length of the 10^{-4} M sample is about equal to the sample thickness, so large variations in the spatial distribution of the luminescence are provided by the five samples. Students enjoy seeing visual confirmation of Beer's law.

Initial oscilloscope measurements are made with the photodiode connected to one vertical input, the PMT output connected to the second vertical input, and the oscilloscope triggered by the photodiode signal. An empty sample tube is placed in the sample block, and the monochromator is tuned to 340 nm so that scattered laser light reaches the PMT. Using this configuration, students measure the time delay between the photodiode and PMT signals. This information is needed to temporally align calculated and observed wave

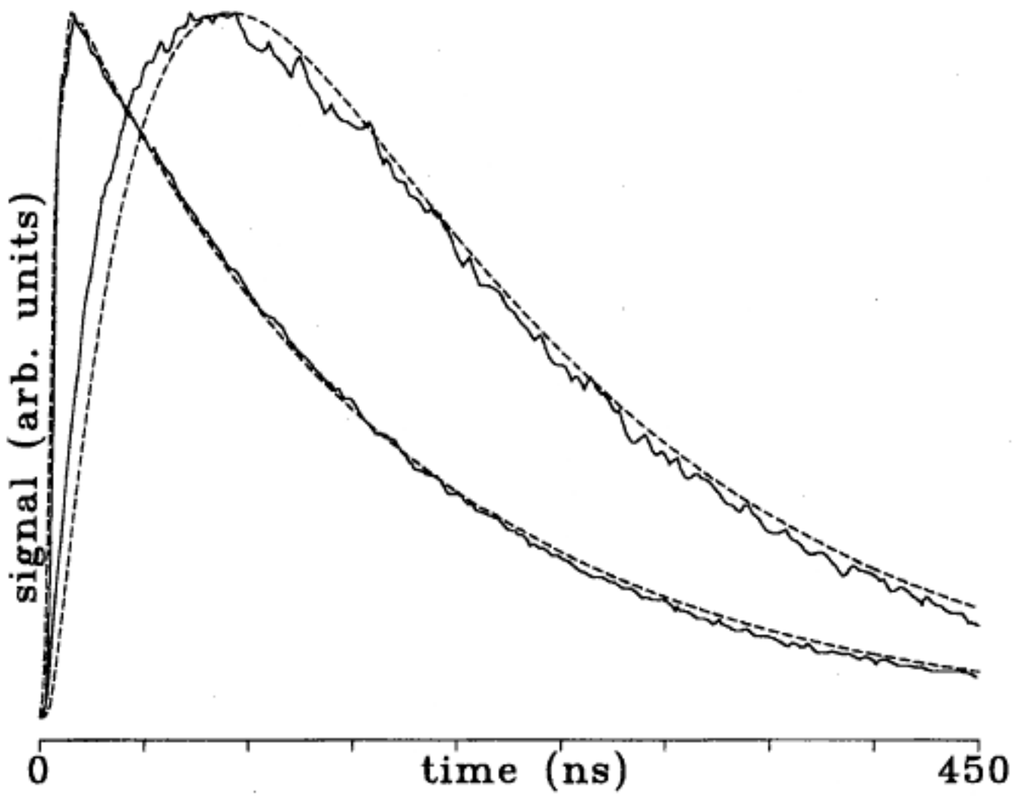

Figure 7. Observed (solid lines) and calculated (dashed lines) P^* and PD^* fluorescence for 10^{-2} M pyrene.

forms in the data analysis. Next, the overall instrument time response is obtained by recording a scattered laser-light signal at each of the three oscilloscope sweep times used to measure pyrene data. These traces are transferred to the PC for later use. Finally, the pyrene luminescence signals are recorded and transferred to the PC.

Table 2 lists approximate settings used for each sample concentration for 400- and 500-nm data. Different PMT voltages are used for each data set, so intensity information is not available. The 10-mV/div vertical sensitivity for the oscilloscope is necessary to insure that the PMT current does not saturate (a 50-mV signal at the 50-Ω input of the oscilloscope requires 1 mA of PMT current).

Figures 2 and 5–7 show raw data from a single laser shot. Digital oscilloscopes contain internal signal-averaging capabilities that can considerably reduce observed noise, although the noise level shown here does not affect students' ability to analyze the data. All of the information required for this experiment can easily be obtained in one 3-h lab period. The analysis described in the next section can either be done during a second lab period or out of class.

Analysis

The simplest analysis procedure assumes a set of rate constants and uses either eqs 10 and 11 or eqs 12 and 13 to calculate P^* and PD^* emission signals. The calculated waveforms are displayed with the experimental data, and students adjust the rate constants until good agreement between calculated and observed signals obtains. However, this procedure will not work directly due to instrument limitations. The response time of the apparatus is restricted by the about 2-ns rise time of the PMT. This behavior is sufficiently fast to reproduce the PD^* signal with relatively little distortion, but recording undistorted P^* data, particularly for the more concentrated samples, is completely unrealistic. This situation provides students with an ideal example of how experimental procedures can introduce errors, and how proper analysis can correct inevitable limitations.

Interactive Data-Analysis Procedure

Convoluting the Calculated Waveform

It is not practical to remove instrument effects from the data, but it is straightforward to subject calculated waveforms to the same distortions as experienced by the emission signals. This is done by convoluting the calculated waveform, $C(t)$, with the instrument response, $P(t)$, which is just the PMT's response to scattered laser light. The instrumentally distorted form of $C(t)$, labelled $D(t)$, is formally given by the convolution integral (*7*),

$$D(t) = \int_0^t C(\tau)P(t-\tau)\mathrm{d}\tau \qquad (14)$$

Because the experimental data and the calculated signal consist of discrete points in time, the convolution integral is replaced by a summation running over the data points.

$$D_t = \sum_{\tau=0}^{t} C_\tau P_{t-\tau} \qquad (15)$$

The affect of this convolution procedure is shown in Figure 5, where curve A is the PMT response, and curve B is the calculated P^* signal for $[P] = 10^{-2}$ M. Curves C are the experimental data (solid) and the convolution of A and B (dashed). Figure 5 makes it quite clear that the convolution process is necessary to compare calculated and observed signals for $[P^*]$. This convolution procedure also makes it possible to carry out this experiment using broader laser pulses or a slower oscilloscope.

Agreement between Calculations and Data

The summation of eq 15 is evaluated in the same computer program used to evaluate the C_t values. The program then displays the D_t waveforms for both P^* and PD^*, along with the experimental data for a given concentration. Students analyze their data by adjusting the rate constants to obtain good agreement between calculations and observed data. It is possible, although rather difficult, to incorporate the convolution procedure into a nonlinear least-squares fitting calculation. However, this form of analysis becomes a blackbox for students, and their appreciation of how the individual rate constants affect the data is lost. The interactive analysis described here gives students a good understanding of how different portions of the data are sensitive to different rate constants.

Excellent agreement can be obtained for each concentration, but some compromises are required to arrive at a single set of rate constants that best describe all data. This can be seen in comparing Figures 6 and 7, which show calculated and observed results for $[P] = 10^{-3}$ and $[P] = 10^{-2}$ M samples. Both figures use

$$k_M = 2.1 \times 10^6$$

$$k_D = 2.3 \times 10^7$$

$$k_{DM} = 2.5 \times 10^6$$

and

$$k_{MD} = 5.0 \times 10^9$$

The first point emphasized by these figures is the dramatic concentration dependence of pyrene luminescence. It is also clear that there is quite good agreement between the calculated and observed curves, but there are small systematic deviations. The most noticeable problem is the excess observed intensity during the initial rise of the excimer signal. No combination of rate constants adequately fits this rise time; an impurity with a short lifetime fluorescence at 500 nm is the probable cause of this feature. One reason a single set of rate constants cannot fit all samples perfectly is found in uncertainties in the sample concentrations. Each solution was prepared carefully, but the degassing process can introduce unknown concentration changes.

Discussion

This experiment has proven to be an effective introduction to a variety of topics in photochemical kinetics and fast-measurement techniques. The combination of simple visual observations, measurements with nanosecond time resolution, and an interactive data-analysis procedure brings together many of the best elements of experimental physical chemistry. The initial onset and the subsequent decay of the excimer concentration play the role of a classic reactive intermediate, and the large value of k_{MD} identifies excimer formation as a diffusion-controlled process. The ability to properly account for inherent instrumental limitations through the convolution procedure is an important lesson in identifying and solving experimental problems.

This experiment interacts well with any work done with a fluorimeter; it has good connections with a phosphorescence emission experiment we use (*8*). The concentrations of the samples could be measured independently with a standard UV–vis spectrophotometer. This study of excimers can also be extended in a number of ways. For example, in contrast to excimer formation involving two identical molecules, excited-state complexes (exciplexes) can also be studied. Pyrene forms an exciplex with dimethyl aniline; this can be studied in much the same manner as pyrene excimers (*9*). In this project, 10^{-6} M pyrene,

which students now know does not form the excimer, reacts with dimethyl aniline to form the exciplex. Wavelength-dependent fluorescence is again used to monitor the time-dependent concentrations of P^* and the exciplex in samples having different aniline concentrations.

In a minimum configuration, the apparatus can be assembled for less than $10,000. The components used are common, general-purpose instruments that already exist in many laboratories; they can be used in a wide variety of experiments. We provide our students with an extensive description of the experiment, including operating instructions. This material also discusses the nitrogen laser in detail and describes precautions necessary for fast electronic measurements. Copies of this material, either on paper or WordPerfect 5.1 floppy disk, and analysis computer programs written in ASYST and QuickBasic are available at no cost from J. Muenter.

Acknowledgment

Financial support from a Kresge Foundation grant is gratefully acknowledged.

Literature Cited

1. Kovalenko, L. J.; Leone, S. R. *J. Chem. Educ.* **1988**, *65*, 681–687.
2. Muenter, J. S. *J. Chem. Educ.* **1996**, 73, 576–580.
3. Schwenz, R. W.; Moore, R. J. *Physical Chemistry: Developing a Dynamic Curriculum*; ACS: Washington, DC, 1993; Chapters 6–13. Galloway, D. B.; Clolkoowski. E. L.; Dallinger, R. F. *J. Chem. Educ.* **1992**, *69*, 79–83. Erskine, S. R.; Bobbit *J. Chem. Educ.* **1989**, *66*, 354–357. Jones, B. T.; Smith, B. W.; Leong, M. B.; Mignardi, M. A.; Winefordner, J. D. *J. Chem. Educ.* **1989**, *66*, 357–358. King, M. E.; Pitha, R. W.; Soutum, S. F. *J. Chem. Educ.* **1989**, *66*, 787–790. Hughes, E., Jr.; Jelks, V.; Hughes. D. L. *J. Chem. Educ.* **1988**, *65*, 1007–1008.
4. Birks, J. B. *Photophysics of Aromatic Molecules*; Wiley Interscience: London, 1970.
5. Birks, J. B.; Christophorou, L. G. *Spectrochim. Acta* **1963**, *19*, 401–410.
6. Eyring, H.; Lin, S. H.; Lin, S. M. *Basic Chemical Kinetics*; Wiley: New York, 1980.
7. Sokolnikoff, I. S.; Redheffer, R. M. *Mathematics of Physics and Modern Engineering*; McGraw–Hill: New York; p 488.
8. Dyke, T. R.; Muenter, J. S. *J. Chem. Educ.* **1975**, *52*, 251–258.
9. Mataga, N.; Okada, T.; Ezumi, K. *Mol. Physics* **1966**, *10*, 203–204.

An Easily Demonstrated Zero-Order Reaction in Solution

Kathryn Hindmarsh and Donald A. House
University of Canterbury, Christchurch, New Zealand

Zero-order reactions are chemical kinetics curiosities. In most text books, they are only briefly mentioned before the discussion rapidly passes to first-order reactions; examples from inorganic chemistry are seldom discussed in detail and are hardly ever illustrated by an example. A rare exception is Fig. 8.3 in Wilkins (*1*) showing the absorbance versuss time plot for the reaction between Cr^{II}_2 and I_3^- at 410 nm (*2*).

Such reactions are easily recognised by **linear** absorbance versus time traces, ending abruptly when the rate limiting reagent is consumed.

We have recently discovered that the oxidation of $PtCl_4^{2-}$ by excess $S_2O_8^{2-}$ in HCl is a reaction exhibiting all the characteristics of a typical zero-order reaction (see figure). Zero-order (linearity) is observed over a wide range of $S_2O_8^{2-}$ concentrations (5–50 mM) with $[PtCl_4^{2-}] = 0.6$ mM and the slope and "end-time" are proportional to $[S_2O_8^{2-}]$. To obtain the figure (Hewlett Packard Diode Array Spectrophotometer, room temperature, 1.0 cm quartz cell, $\lambda = 340$ nm), equal volumes (1.0 mL) of 1.2 mM (25 mg/50 mL) K_2PtCl_4 in water and 100 mM $Na_2S_2O_8$ (0.596 g/25 mL) in 2 M HCl were mixed in the spectrophotometer cell and the absorbance versus time mode of the spectrophotometer was activated (one data point every 100 s for 1 hr). Other spectrophotometers (Perkin Elmer λ2) give equally satisfactory data. It is important that the $S_2O_8^{2-}$ solution be freshly prepared, but the Pt(II) solution is stable for at least 2 weeks in the dark.

Obviously, the rate law is

$$d\,[Pt(II)]/d\,t = k_o[S_2O_8^{2-}] \quad (1)$$

and with excess $S_2O_8^{2-}$,

$$d\,[Pt(II)]/d\,t = k^{\circ}_{obs}\ (M\ s^{-1}) \quad (2)$$

where

$$k_o = k^{\circ}_{obs}[S_2O_8^{2-}]^{-1} \quad (3)$$

but very little else is known about the reaction.

Oxidations using $S_2O_8^{2-}$ have a propensity for zero-order kinetics (*3*) (for example, with $C_2O_4^{2-}$, HCO_2^-, ROH, and $S_2O_3^{2-}$), and a mechanism involving a steady state concentration of SO_4 radicals is probable.

Literature Cited

1. Wilkins, R.G. *Kinetics and Mechanism of Reactions of Transition Metal Complexes*; VCH: Weinheim, Germany, 1991; p 382,
2. Wilson, L. M.; Cannon, R.D. *Inorg. Chem.* **1985**, *24*, 4366.
3. House, D. A. *Chem. Rev.* **1962**, *62* , 185.

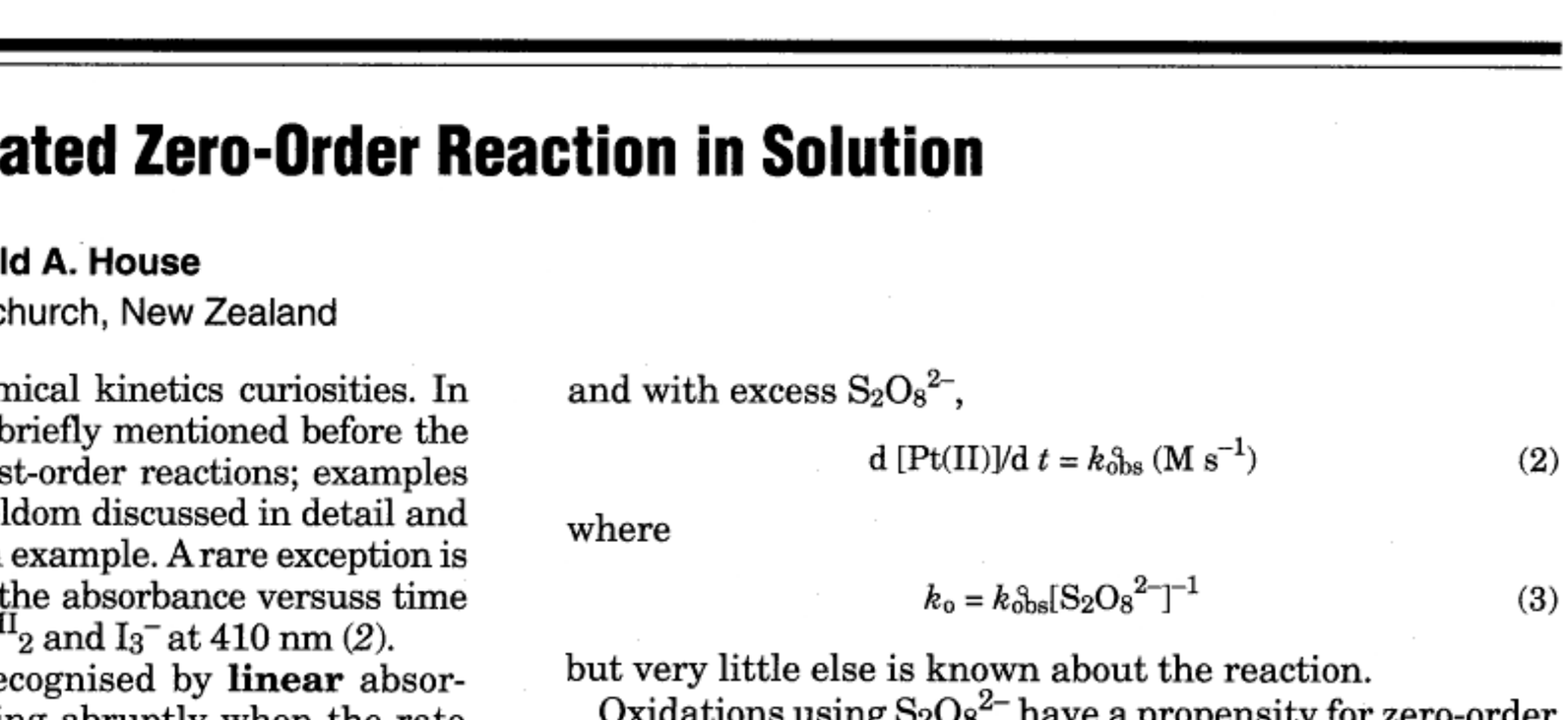

Absorbance vs time trace for the reaction between $S_2O_8^{2-}$ and $PtCl_4^{2-}$. $[S_2O_8^{2-}] = 50$ mM, $[PtCl_4^{2-}] = 0.6$ mM, [HCl] = 1.0 M, room temperature.